NUMERICAL INVESTIGATION OF HEAT TRANSFER FROM A PLANE SURFACE DUE TO ANNULAR SWIRLING TURBULENT JET IMPINGEMENT

Farhana Afroz and Muhammad A.R. Sharif
Aerospace Engineering and Mechanics Department, The University of Alabama
Tuscaloosa, AL35487-0280, United States

ABSTRACT

This paper presents numerical study of heat transfer characteristics of an annular turbulent swirling jet impingement on a plane heated surface. Annular jet configuration causes instabilities and fluctuations in the flow and depending on the combinations of different parameters, the annular jet impingement may have positive or negative effects on the heat transfer rate over impingement surface. On the other hand, swirl introduces vorticity and fluid mixing in impinging jet, which is desirable in some applications. Axisymmetric two-dimensional flow domain with and without swirling flow is considered in this study. The Realizable k-epsilon turbulence model with enhanced wall treatment is used in the computation. Earlier studies on turbulent swirling impinging jet flow configuration demonstrated superior performance of this turbulence model. The numerical computations are conducted using the ANSYS Fluent code. The computational process is validated against other published data on similar flow configuration for non-swirling and swirling annular impinging jets. The flow and geometric parameters are the jet exit Reynolds number, Re, the swirl strength Sw, the jet exit to target surface distance, H, and the blockage ratio of the annular jet, B. Various combinations of these parameters are considered and the thermal-hydraulic field in the domain is computed. The effects of these parameters on the Nusselt number distribution on the impingement surface is investigated. This study will help to understand the complex flow behavior of the swirling annular jet impingement and help to find the optimal combinations of the different parameters to obtain the desired heat transfer distribution on impingement surface as well as the desired level of fluid mixing.

1. INTRODUCTION

Impinging jet heat transfers are widely used in many industrial applications like heating, cooling and drying applications. The jets are usually issued from circular nozzle or rectangular slots and impinged on the target surface. By inserting a coaxial rod inside a circular tube a special configuration of jet flow can be achieved which is known as "annular jet". Although an extensive research study has been conducted on heat transfer from round jets or slot jets impingement but inadequate research has been done on heat transfer characteristics from such annular jet configurations.

Earlier research works on annular jet includes the experimental study of turbulent annular jet conducted by Maki and Ito[1] and Maki and Yabe[2]. Their studies revealed that for shorter jet-to-target distance, a reverse stagnation flow can occur towards the jet axis. The local heat transfer and pressure coefficient along the impingement surface can be severely affected by this reverse flow.

One recent experimental work was performed to analyze the effect of diameter ratio of annular nozzle ($0.5 \leq D_i/D_o \leq 1.0$), Reynolds number ($3{,}000 \leq Re \leq 10{,}000$), and jet-to-target separation distance ($1.0 \leq H/D \leq 2$) on heat transfer (Ichimiya[3]). Heat transfer rate increases when Reynolds number and diameter ratio is fixed but separation distance decreases. Also if the Reynolds number and separation distance increases but the diameter ratio decreases, then the stagnation heat transfer increases.

Experimental and numerical investigation of annular jet impinging at Re = 20,000, based on outer diameter and average velocity for a diameter ratio of 0.44, shows that impinging jet heat transfer is higher than conventional round jet at low jet-to-target distance (H/D = 2.0) (Musika et al.[4]). Another experimental study identified that annular nozzle causes instabilities and turbulent fluctuations in the downstream axial zone compared to the circular jet and can enhance impinging heat transfer (Kalinina et al.[5]).

Swirling at jet exit can be an important parameter that influences impinging heat transfer. The local Nusselt number along the hot impinging surface due to a round swirling jet was investigated for Re = 23,000 and H/D = 2, 6 and 10 (Lee et al.[6]). The swirling strength, SW was varied here up to 0.77 and average Nusselt number for swirling jet was higher than non-swirling jet at H/D = 2.0. For H/D = 6 and 10, the average Nusselt number was higher at low swirling strength (≤ 0.21) and was lesser at high swirling strength (> 0.21) compared to the non-swirling jets.

The combined effect of swirling and annular configuration on impinging jet heat transfer would result in complex and interesting flow structure. It might have positive or negative effect on heat transfer depending on combinations of different parameters. Very few studies have been done so far on impinging heat transfer due to annular jet with swirling. A recent experimental study investigated annular jet characteristics with/without swirling (Yang et al.[7]).The annular jet was diameter ratio D_i/D_o = 0.5 and the Reynolds number was 7,000. The swirling strength was 0.92 and at short and intermediate jet-to-target separation distances, more non-uniform heat

transfer and pressure coefficient along the hot impinging surface was found for swirling annular jet as compare to non-swirling annular jet. For, larger jet-to-target separation distances, the opposite scenario occurred.

As the majority of research work has been conducted on either annular jet or swirling round jet, more research effort are needed to explore the combined effect of annular jet and swirling on impinging jet heat transfer.

The aim of the present study is to vary the swirling strength and jet-to-target separation distance and see the flow structure and heat transfer characteristics of an annular turbulent impinging jet. But the other parameters including Reynolds number and diameter ratio are kept fixed in this study.

2. PROBLEM DESCRIPTION

In the present study, annular pipe has inner diameter of D_i = 0.0225 m and outer diameter of D_o = 0.03 m. So the jet diameter ratio or blockage ratio, D_i/D_o = 0.75. The Reynolds number, Re = 5,000 for all numerical analysis is calculated based on inlet velocity, U_{in} and D. The non-dimensional separation distance, H/D is varied from 0.5 to 8 and swirling strength, SW (defined later) is varied from 0 to 1. The height and length of the computational domain is $10D_o$ X $10D_o$ and the literature supports that this length is adequate to eliminate the end effect(Laschefski et al.[8]).

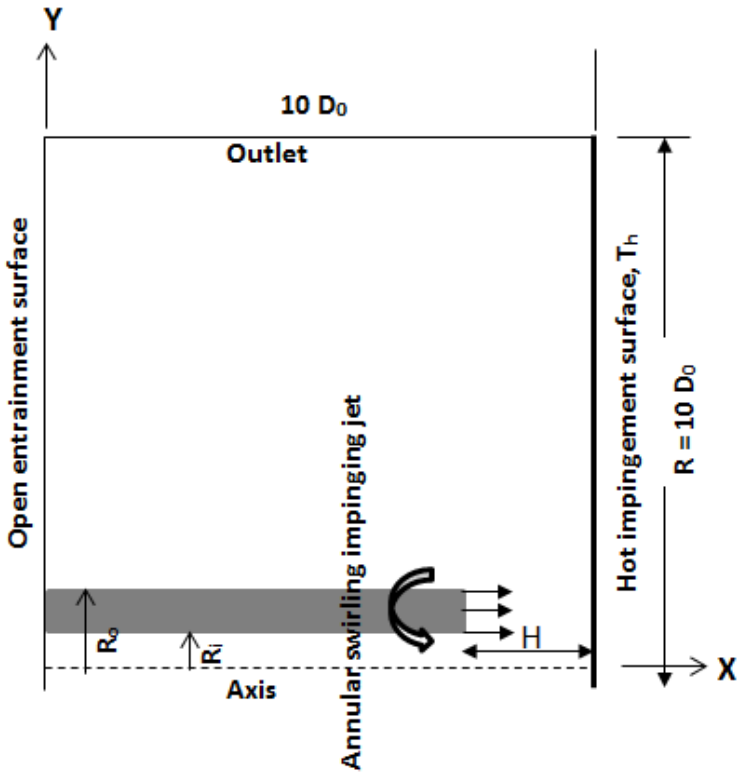

Figure 1 Schematic diagram of annular swirling impinging jet

3. NUMERICAL PROCEDURE

3.1 Governing mathematical equations

The governing equations in this current study are conservation of mass, momentum, and energy. The equations are expressed in terms of the cylindrical coordinate system with constant fluid properties:

Continuity equation

$$\frac{\partial \mathrm{u}}{\partial \mathrm{x}} + \frac{1}{\mathrm{y}}\frac{\partial(\mathrm{yv})}{\partial \mathrm{y}} = 0 \tag{1}$$

Momentum equation

$$\frac{\partial \mathrm{u}^2}{\partial \mathrm{x}} + \frac{1}{\mathrm{y}}\frac{\partial(\mathrm{vu})}{\partial \mathrm{y}} = -\frac{1}{\rho}\frac{\partial \mathrm{p}}{\partial \mathrm{x}} + \frac{\partial(\tau_{\mathrm{xx}})}{\partial \mathrm{x}} + \frac{1}{\mathrm{y}}\frac{\partial(\tau_{\mathrm{xy}})}{\partial \mathrm{y}} \tag{2}$$

$$\frac{\partial(\mathrm{uv})}{\partial \mathrm{x}} + \frac{1}{\mathrm{y}}\frac{\partial(\mathrm{yv}^2)}{\partial \mathrm{y}} = -\frac{1}{\rho}\frac{\partial \mathrm{p}}{\partial \mathrm{y}} + \frac{\partial(\tau_{\mathrm{xy}})}{\partial \mathrm{x}} + \frac{1}{\mathrm{y}}\frac{\partial(\mathrm{y}\tau_{\mathrm{yy}})}{\partial \mathrm{y}} - \frac{\tau_{\mathrm{zz}}}{\mathrm{y}} \tag{3}$$

$$\frac{\partial(\mathrm{uw})}{\partial \mathrm{x}} + \frac{1}{\mathrm{y}}\frac{\partial(\mathrm{yvw})}{\partial \mathrm{y}} - \frac{\mathrm{vw}}{\mathrm{y}} = \frac{\partial(\tau_{\mathrm{xz}})}{\partial \mathrm{x}} + \frac{1}{\mathrm{y}^2}\frac{\partial(\mathrm{y}^2\tau_{\mathrm{yz}})}{\partial \mathrm{y}} \tag{4}$$

Energy equation

$$\frac{\partial(\mathrm{uT})}{\partial \mathrm{x}} + \frac{1}{\mathrm{y}}\frac{\partial(\mathrm{yvT})}{\partial \mathrm{y}} = \frac{1}{\rho \mathrm{c_p}}\left[\frac{\partial(\mathrm{q_x})}{\partial \mathrm{x}} + \frac{1}{\mathrm{y}}\frac{\partial(\mathrm{yq_y})}{\partial \mathrm{y}}\right] \tag{5}$$

where *u*, *v*, and *w* are axial (*x*), radial (*y*), and azimuthal (*z*) the velocity components, *p* is the pressure, and *T* is the temperature. Here, constant fluid density and specific heat at constant pressure are represented by ρ and c_p. The stress terms in Eqs. (2) – (4) are written in terms of the velocity gradients as

$$\tau_{\mathrm{xx}} = 2\nu\frac{\partial \mathrm{u}}{\partial \mathrm{x}}, \tau_{\mathrm{yy}} = 2\nu\frac{\partial \mathrm{v}}{\partial \mathrm{y}}, \tau_{\mathrm{zz}} = 2\nu\frac{\mathrm{v}}{\mathrm{y}},$$

$$\tau_{\mathrm{xy}} = \tau_{\mathrm{yx}} = \nu\left(\frac{\partial \mathrm{v}}{\partial \mathrm{x}} + \frac{\partial \mathrm{u}}{\partial \mathrm{y}}\right), \tau_{\mathrm{yz}} = \tau_{\mathrm{zy}} = \nu\left(\frac{\partial \mathrm{w}}{\partial \mathrm{y}} - \frac{\mathrm{w}}{\mathrm{y}}\right), \tau_{\mathrm{zx}} = \tau_{\mathrm{xz}} = \nu\left(\frac{\partial \mathrm{w}}{\partial \mathrm{x}}\right)$$

where ν is kinematic viscosity and the turbulent heat fluxes in Eq. (5) are expressed in terms of the temperature gradient as

$$\mathrm{q_x} = \mathrm{k}\frac{\partial \mathrm{T}}{\partial \mathrm{x}}, \mathrm{q_y} = \mathrm{k}\frac{\partial \mathrm{T}}{\partial \mathrm{y}}.$$

where *k* is the fluid thermal conductivity.

The Reynolds number is expressed as $\mathrm{Re} = U_{in}D/\nu$ and and Prandtl number $\mathrm{Pr} = \nu/\alpha$, where α represents the fluid thermal diffusivity.

On the hot impingement surface the local Nusselt number is defined as

$$\mathrm{Nu} = \frac{\dot{q}D}{k(T_h - T_c)} \tag{6}$$

where the surface heat flux is represented by $\dot{q}$.

The swirl number, SW, at the jet exit is defined as the ratio of the azimuthal momentum (G_z) to the axial momentum (G_x),

$$\mathrm{SW} = \frac{G_z}{G_x} = \frac{\int_{\text{jet exit}} \rho u w \, (y dy)}{\int_{\text{jet exit}} \rho u u \, (y dy)} \tag{8}$$

In practical applications, the jet exit swirl is imposed by using swirl generator vane or inserting a twisted tape inside jet pipe. Thus, if the swirl velocity information at the jet exit is not accessible for a specific swirl guide vane or twisted tape, then numerically it is very challenging to impose swirl velocity at jet exit. A simple substitute method is to impose a rigid body rotation as $w = y\omega$ at the jet exit, where ω is a constant angular speed. Thus, Eq. (8) with uniform jet exit axial velocity U_{in} can be written as

$$\mathrm{Sw} = \frac{\omega}{U_{in}} \frac{\int_{D_i/2}^{D_o/2} y^2 dy}{\int_{D_i/2}^{D_o/2} y dy} = \frac{1}{3} \frac{\omega (D_o - D_{i)}}{U_{in}} \qquad \text{or} \qquad \omega = 3 \, \mathrm{Sw} \, U_{in} / (D_o - D_{i)} \tag{9}$$

3.2 Computational details

All the computations are conducted using commercial software ANSYS Fluent 17.2. Integration over the finite volume meshes produces a set of linear equations. The coupling between pressure and velocity is attained by the SIMPLE method. The normalized residual for solving governing equations is set to 10^{-6} and also the total heat flux at the impingement surface is monitored until it convergences. A sample mesh is shown in Figure 2and the mesh is clustered toward the bottom wall with a bias factor. From edge of jet to top wall the mesh is also clustered with a bias factor but mesh has uniform grid between the axis and jet edge.

3.3 Boundary conditions

The numerical domain in this study is axi-symmetric, at axis of symmetry as shown in bottom boundary (Figure 1). The top boundary is set as outlet and left boundary (excluding the jet inlet) is set as open entrainment boundary. A constant pressure condition is applied on outlet and open entrainment boundary. A uniform velocity, U_{in} at the inlet boundary of annular jet is quantified based on jet exit Reynolds number. The reference length for Reynolds number is annular jet outer diameter, D_0 and the temperature of cold jet, T_c is fixed to 300 K. The right boundary of this domain is hot circular impingement surface which has constant temperature, T_h of 315 K. The value of SW, at inlet is set as rigid body rotation.

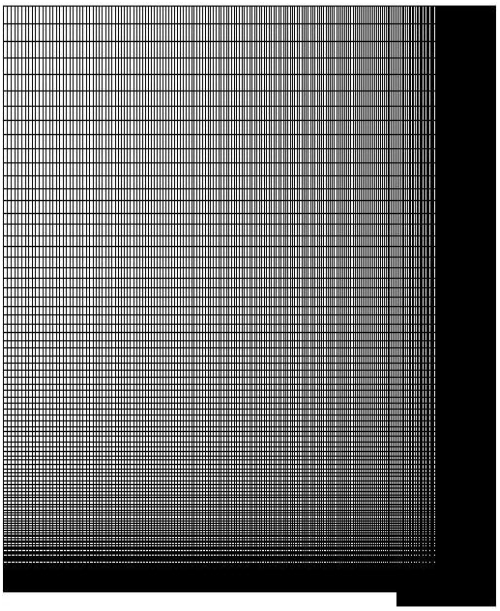

Figure 2 Sample mesh of annular jet.

3.4 Turbulence model validation

The local Nusselt number along the hot impingement plate for Re = 20,000, SW = 0 and D_i/D_o = 0.44, and H/D = 2.0 is compared with the experimental data of Musika et al.[4]. Four different Turbulence models including RNG-k-ε model, Realizable k-ε model, Transition SST model and Reynolds stress model are used to compute the local Nusselt number and compared with experimental data to identify the appropriate numerical model for present study (Figure 3). Among the four different turbulence models, prediction of local Nusselt number by Realizable k-ε model gives better agreement and thus used for present simulation.

The Realizable k-ε turbulence model is used to validate the pressure coefficient data along the hot impingement surface against the experimental data (Yang et al.[7]) for Re = 7,000, SW = 0 and D_i/D_o = 0.5, and for two separation distance H/D = 0.5 and H/D = 4.1 (Figure 3). The comparison shows very good agreement and thus proves that this turbulence model is reliable for predicting heat transfer and flow structure of annular impinging jet model.

3.5 Grid refinement study

A systematic mesh refinement study is present in Figure 4. It can be seen that there is no significant change in local Nusselt number beyond the mesh resolution of 180 X 127 and thus this mesh resolution is used for all numerical simulations with H/D = 2.0.The mesh resolutions for other separation distances of H/D are adjusted proportionally. The plot for Y+ along the hot impingement surface for 180 X 127 mesh shows that majority of $Y+$ value stays below 2. So very fine mesh requirement near wall for Realizable k-ε turbulence model is also satisfied.

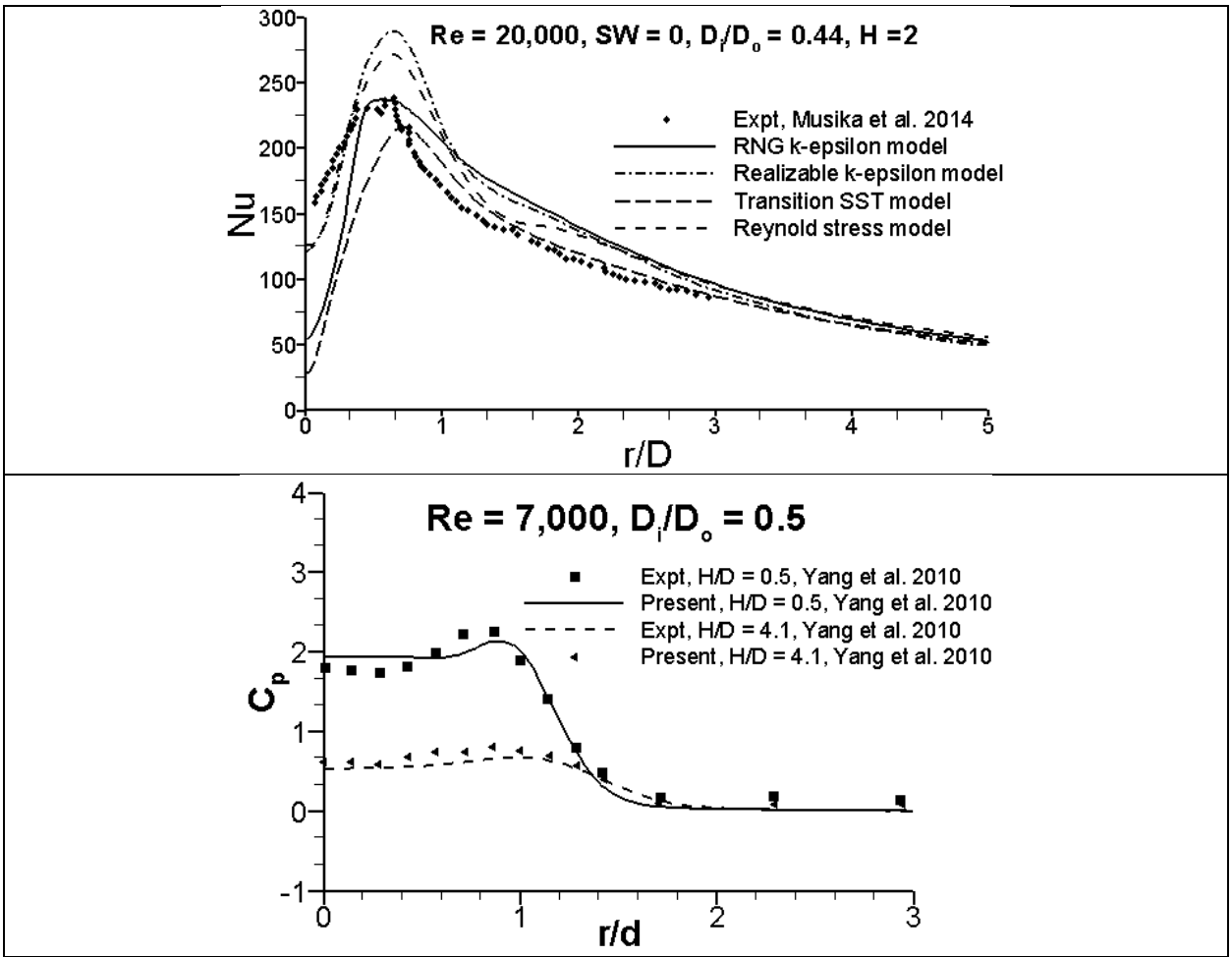

Figure 3. Comparison of local Nusselt number and pressure coefficient along the hot impingement surface against experimental data.

4. RESULTS AND DISCUSSIONS

4.1 Annular Impinging jets

4.1.1 Pressure coefficient and local Nusselt number distribution

The value of *H/D* is varied from 0.5 to 8, while Re = 5,000, D_i/D_0 = 0.75 is remain fixed. The effect of varying the separation distance, *H/D* on local Nusselt number and pressure coefficient distribution in the radial direction along the hot impingement surface is presented in Figure 5. The separation distance strongly influences pressure coefficient and Nusselt number. Basically, there are three different separation distance ranges which affect the Nusselt number and pressure coefficient distribution differently are summarized below.

Range 1: $0.5 \le H/D \le 1.35$: At this shorter separation distance range, the local Nusselt number and pressure distribution shows that flow diverges outside of the slot. The peak of Nu and C_P is

maximum for *H/D* = 0.5 and as separation distance increases, the stagnation point moves further downstream away from jet axis. At, *H/D* = 1.35, the peak Nu and C_P radially shifts to outward direction at a location about *r/D* = 0.9. In this range, value of Nu and C_P in central region near the symmetry axis(*r/D* = 0) is very low compare to larger separation distance (*H/D* ≤ 1.4). The peak value Nu and C_P also decreases monotonically with increasing separation distance.

Range 2: 1.4 ≤ *H/D* ≤ 2.0 At this intermediate separation distance range, the peak Nu and C_P is located near the jet axis but inside the slot. The value if Nu and C_P at symmetry axis(*r/D* = 0) increases with increase of separation distance.

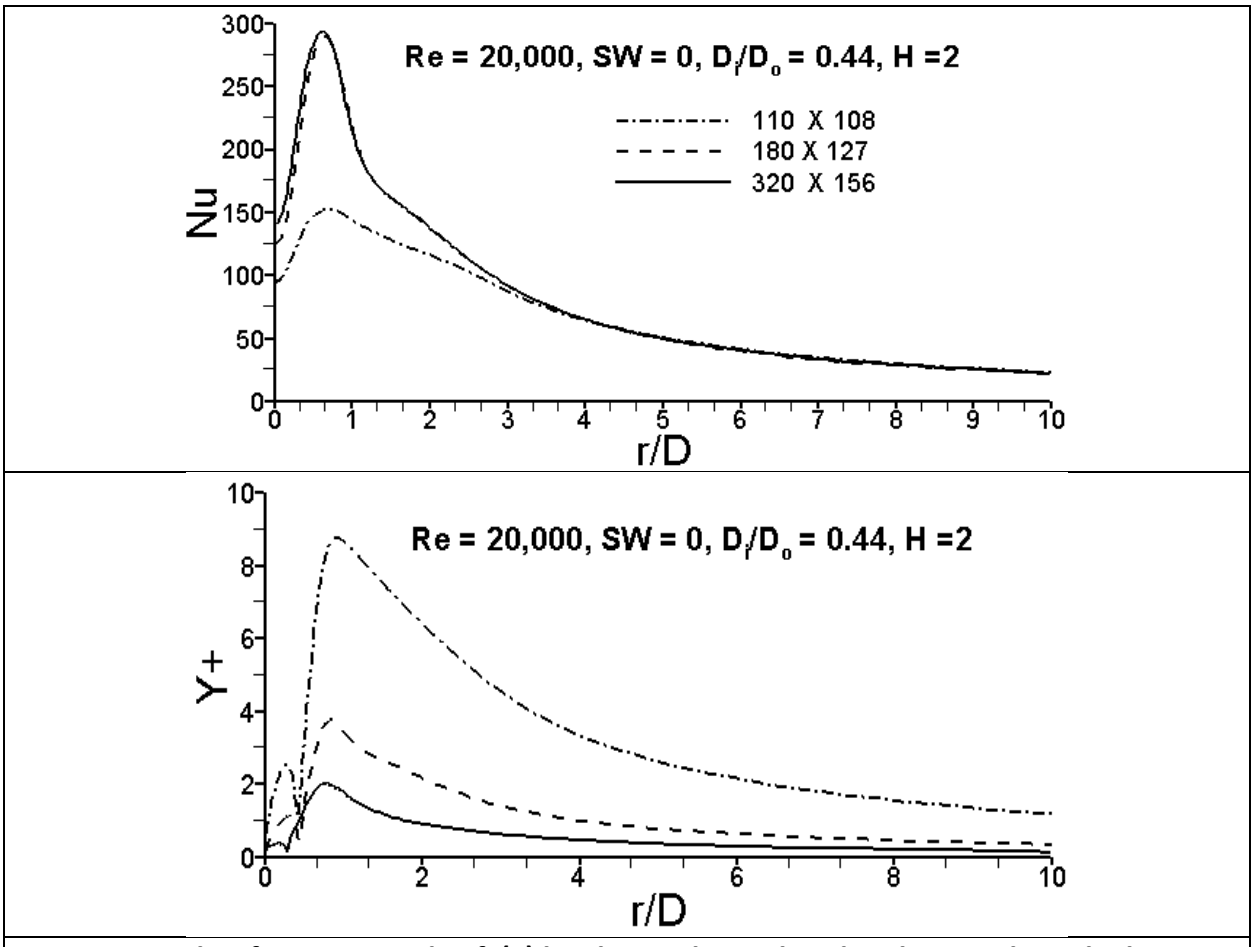

Figure 4. Mesh refinement study of (a) local Nusselt number distribution along the hot impingement surface and (b) distribution of wall y+ along the hot impingement surface.

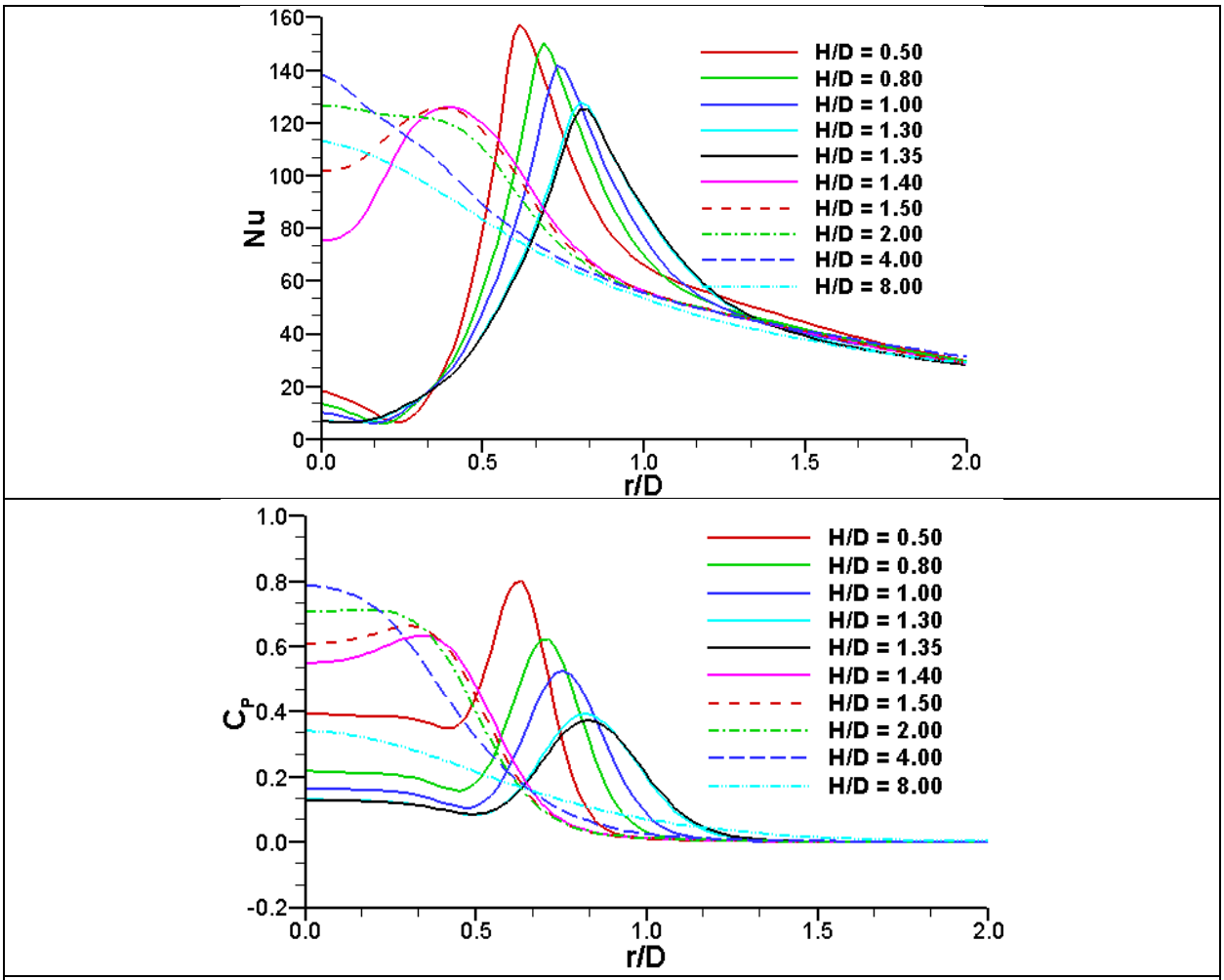

Figure 5. Local Nusselt number and pressure coefficient along radial direction on the hot plate at different jet-to-plate separation distance, *H/D* for Re = 5,000, D_i/D_0 = 0.75.

Range 3: *H/D* > 2.0. At this larger separation distances, the Nu and C_P distribution along the radial direction of hot impingement surface is one of those regular round jet-stagnation flow. The peak of Nu and C_P lie on the symmetry axis (*r/D* = 0), similar to the simple round jet impingement and the heat transfer reduces with increase of separation distance.

4.1.2 Flow hydrodynamics

Figure 6 presents velocity streamlines from each of the threes separation distance ranges that are mentioned in the section 4.1.1. For the shorter separation distance (*H/D* = 0.5, 1.35), the recirculation zone stays on the hot impingement surface which indicates the existence of reverse flow region and the flow is also diverges to the outer side of slot. This flow pattern is flow pattern-2 by Maki and Yabe[2] and the corresponding separation distance where this transition occurs is known as first critical distance. The value of first critical distance here is *H/D* = 1.35 and the flow pattern at 1.4 ≤ *H/D* ≤ 2.0 is known as flow pattern-1, where the

recirculation flow region locates just below the jet exit and flow slightly diverges towards the jet axis. The presence of reverse stagnation point on impingement surfaces causes the lower value of Nu and C_P on the symmetry axis (r/D = 0) in the range of $H/D \geq 1.35$ as seen in Figure 5. As, separation distance increases further, the features of annular jet impingement disappears and

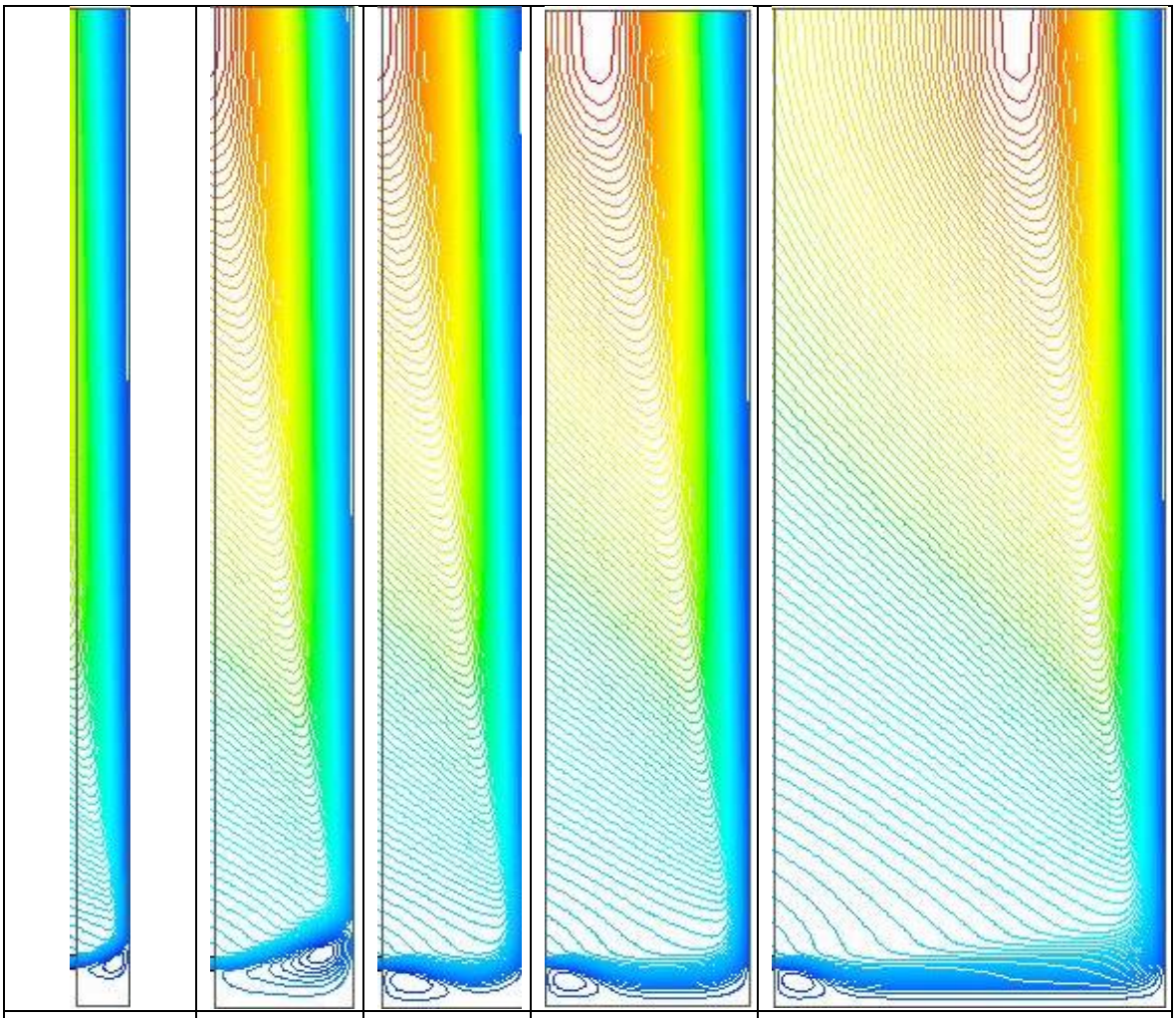

Figure 6. Streamline contour on axial-radial plane for different jet-to-plate separation distance, *H/D* for Re = 5,000, D_i/D_0 = 0.75.

streamline patterns are similar to that of regular round jet impingement($H/D \geq 4$) .

4.2 Annular impinging jet with Swirling

4.2.1 Effect of swirling on pressure coefficient and local Nusselt number distribution

The swirling strength, SW is varied from 0 to 1.0 and corresponding pressure coefficient and Nusselt number distribution along the radial direction on hot impingement surface for intermediate separation distance (H/D = 2.0) and larger separation distance (H/D = 4.0 and 8.0) are present in Figure 7.

C_P	Nu
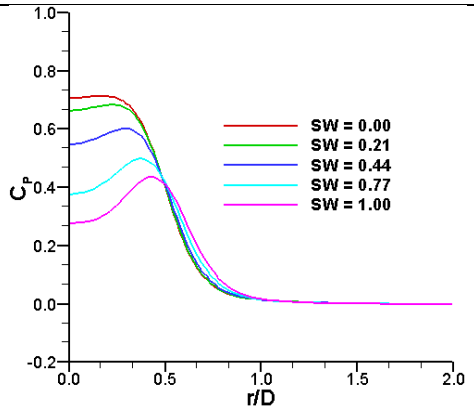	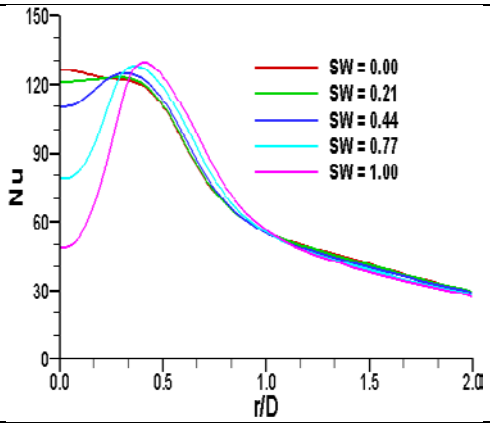
Re = 5,000, H/D = 2.0, D_i/D_0 = 0.75	
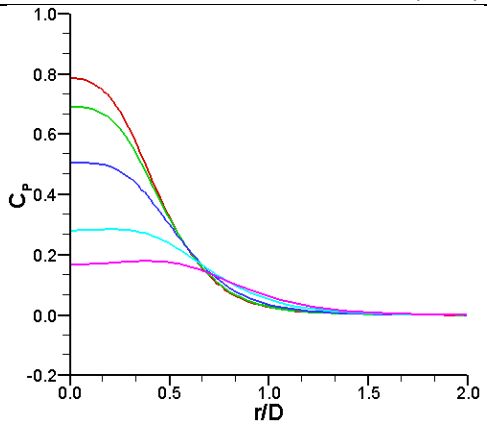	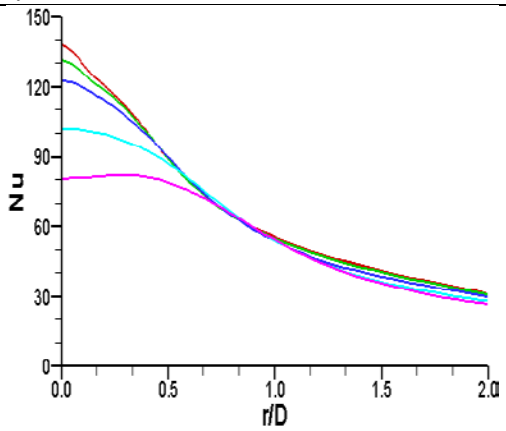
Re = 5,000, H/D = 4.0, D_i/D_0 = 0.75	
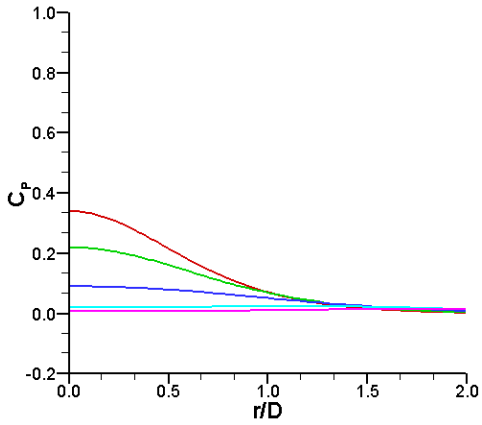	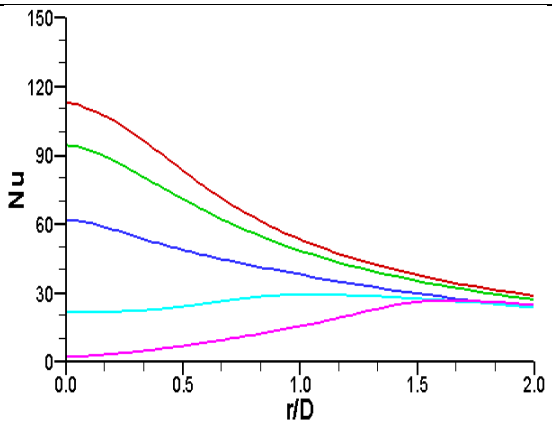
Re = 5,000, H/D = 8.0, D_i/D_0 = 0.75	

Figure 7.Pressure coefficient and local Nusselt number along radial direction on the hot plate at different jet-to-plate separation distance, *H/D*.

For the intermediate separation distance, *H/D* = 2.0, the lower swirling strength, SW = 0.21 cause more uniform, flatten local Nusselt number and pressure coefficient distribution. As SW increases further, the value of Nu and C_P decreases monotonically at the symmetry axis (*r/D* = 0). The Nu and C_P peak radially shifts in downstream direction as SW increases. The peak value of Nu increases with increase of SW but peak of C_P decreases with increase of SW. For larger separation distance (*H*/*D* = 4.0 and 8.0), the overall distribution of Nu and C_P decreases monotonically with increase of SW but also results in more uniform distribution. But exception happens in the case of *H/D* = 8.0, where significant reduction of heat transfer as well as non-uniform distribution occurs for higher swirling strength (SW ≥ 0.77).

4.2.2 Effect of swirling on exit velocity profiles

To evaluate the effect of swirling on flow structures, the radial profile of axial velocity in a selected axial plane (*X/D* = 0.25) is presented in Figure 8. For, intermediate separation distance (*H*/*D* = 2.0), the centerline axial velocity is significantly reduced and peak of axial velocity is located at a downstream location. With increase of *SW*, the centerline axial velocity and peak axial velocity decreases. The higher swirling strength also shifts the peak axial velocity further downstream. At *SW* =1.0, the centerline axial velocity is negative that indicates the presence of reverse flow. For, larger separation distances (*H/D* = 4.0 and 8.0), the axial velocity along radial direction reduces monotonically downstream from symmetry line (*r/D* = 0) and higher swirling strength cause more uniform distribution of axial velocity along the radial direction. But increase of swirl strength strength also reduces overall value of axial velocity and SW ≥ 0.77 results negative axial velocity for the case of *H/D* = 8.0.

4.2.3 Effect of swirling at shorter jet-to-target separation distance

Figure 9 shows the effect of swirling on heat transfer, pressure coefficient and radial profile of axial velocity. It can be seen that axial velocity goes to a negative value because of the presence of reverse stagnation point. Swirling does not show any significant positive or negative contribution on heat transfer for shorter separation distances.

4.2.4 Effect of swirling on flow hydrodynamics

Figure 10 and Figure 11 show the streamlines, swirl velocity contours and isotherms for some representative cases. The air jet from annular nozzle impinges the hot surface and then forms a radial wall jet. The effect of swirl on jet is not that noticeable in these figures of swirl velocity contours. As seen from the streamlines, with increase of swirl strength, the recirculation bubble underneath the jet exit grows bigger in size and drives the flow out slightly to a downstream position. For this reason, the isotherms show that higher swirling strength causes thicker thermal boundary layer near the jet axis.

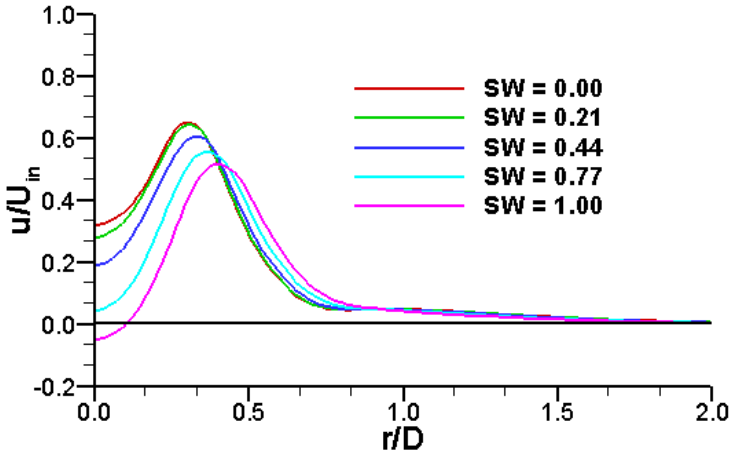

Re = 5,000, H/D = 2.0, D_i/D_0 = 0.75, X/D = 0.25

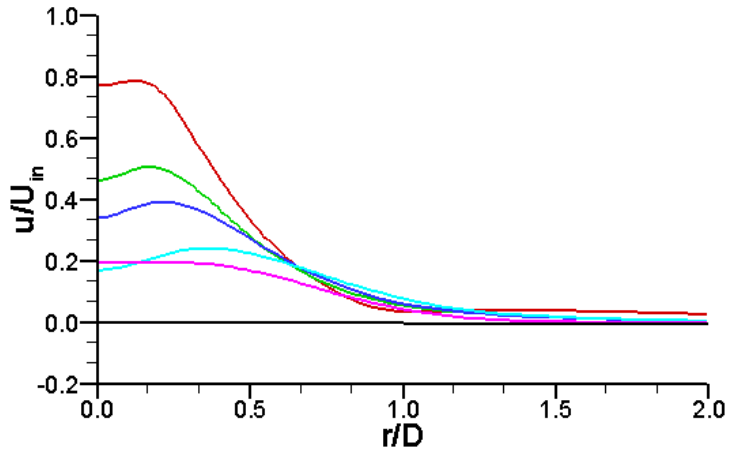

Re = 5,000, H/D = 4.0, D_i/D_0 = 0.75, X/D = 0.25

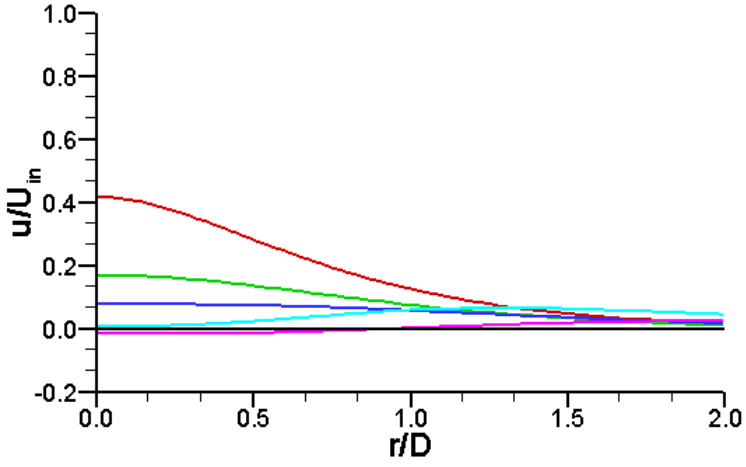

Re = 5,000, H/D = 8.0, D_i/D_0 = 0.75, X/D = 0.25

Figure 8. Comparison of axial component of velocity distribution along the radial direction for *X* = 0.25 *H* for different swirling number.

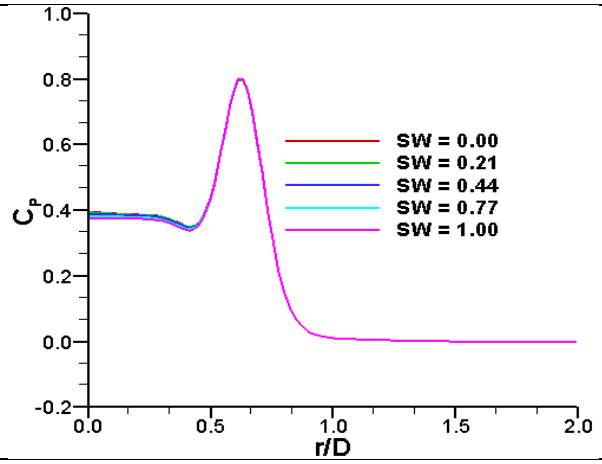

(a)

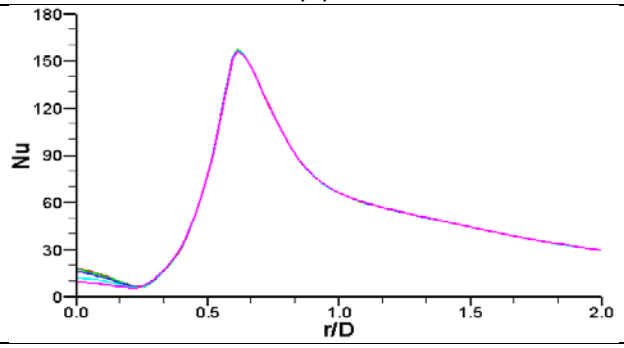

(b)

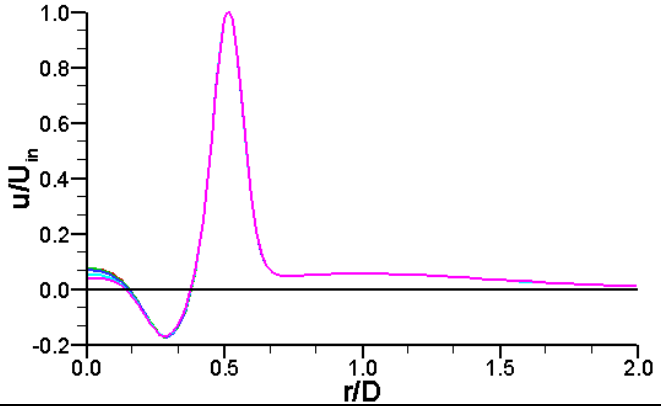

(c)

Figure 9. Distribution of (a) pressure coefficient, (b) local nusselt number,and (c) axial component of velocity along radial direction hot plate for Re = 5,000, *H/D* = 0.5, D_i/D_0 = 0.75.

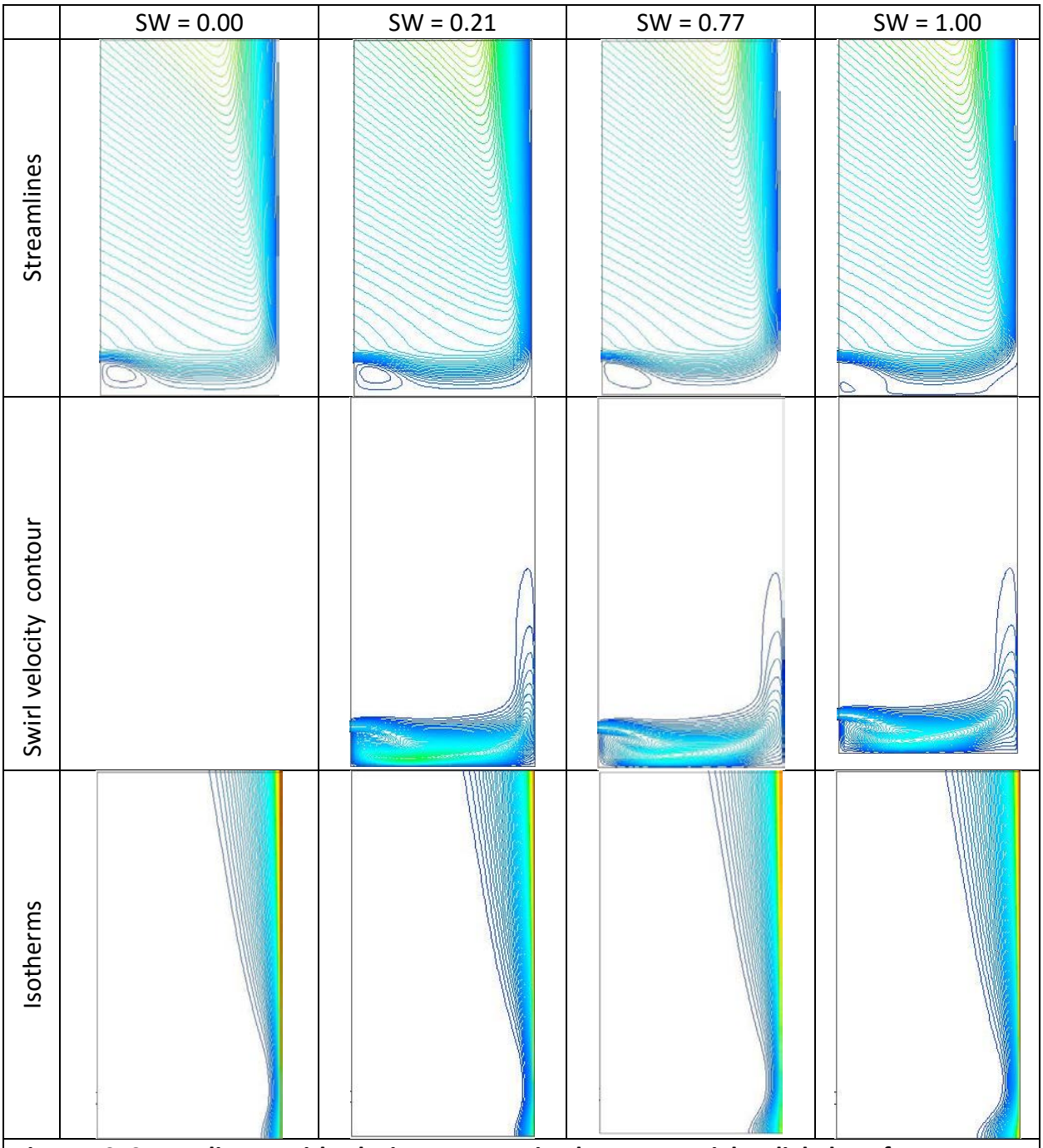

Figure 10. Streamlines, swirl velocity contours, isotherms on axial-radial plane for Re = 5,000, H/D = 2.0, D_i/D_0 = 0.75.

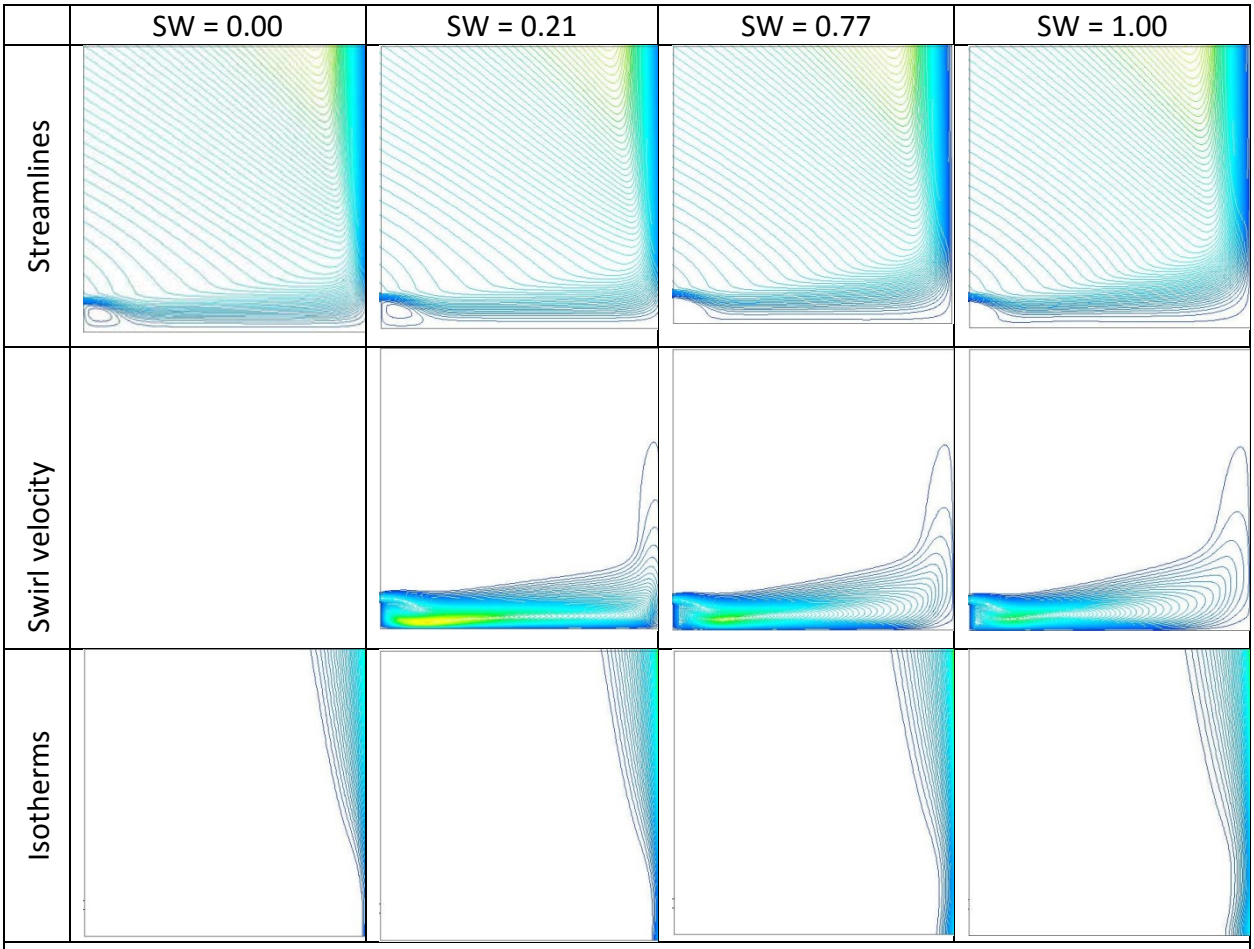

Figure 11. Streamlines, swirl velocity contours, isotherms on axial-radial plane for Re = 5,000, H/D = 4.0, D_i/D_0 = 0.75.

4.2.5 Effect of swirling on heat transfer

Average Nusselt number and stagnation point Nusselt number for different separation distance and swirl strength are presented in Figure 12. Swirling does not affect much on Average Nusselt number and stagnation point Nusselt number for shorter separation distance, H/D = 0.5 and intermediate separation distance, H/D = 2.0. For larger separation distances H/D = 4.0, stagnation point Nusselt number and average Nusselt number both decreases monotonically with increase of swirling strength. But as separation distance gets as high as, H/D = 8.0, average Nusselt number and the peak Nusselt number decreases more abruptly with increase of swirling strength.

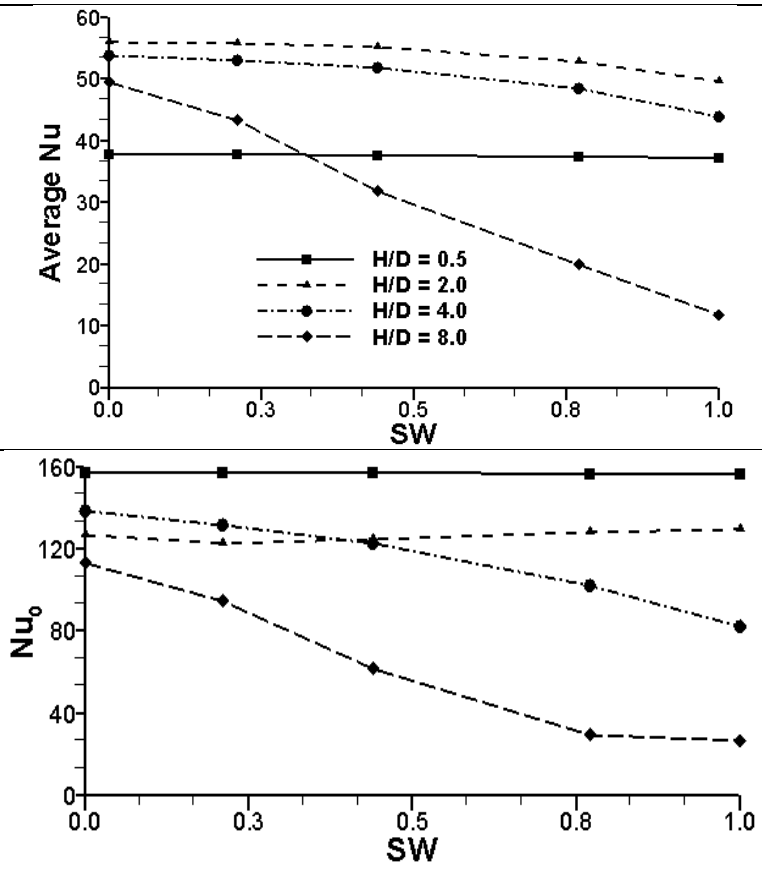

Figure 12.Effect of swirling on variation of average Nusselt number and stagnation point Nusselt number, Nu_0, for various jet-to-plate separation distances.

5. CONCLUSION

Numerical investigation of annular turbulent swirling jet is conducted in this study. The Realizable k-ε model turbulence model is chosen after validating against previously published experimental data. The flow Reynolds number is 5,000 based on the jet exit velocity and annular jet outer diameter and the annular nozzle diameter ratio, D_i/D_o is 0.75. The jet-to-target separation distance, *H/D* is varied from 0.5 to 8 and swirl strength, SW is varied from 0 to 1. The streamlines, isotherms, swirl velocity contour, local Nusselt number and pressure coefficient distribution on hot surface for various combinations of *H/D* and SW are presented. Summary of the results are as follows:

1. Three different jet-to-target separation distance ranges are identified and each range of separation distances affects flow structure and heat transfer differently.

2. Shorter jet-to-target separation distances cause reverse stagnation flow, which has severe negative effect on heat transfer. Imposed swirling motion does not improve the reverse stagnation flow and does not offer any improvement of heat transfer and flow structure.

3. In general, the swirling motion causes the pressure coefficient and Nusselt number distribution more uniform as compared to the non-swirling annular jets for large separation distances. At very large separation distance (*H/D* =8.0), the imposed higher swirl strength (SW ≥ 0.77) motion causes reverse stagnation flow and heat transfer reduces drastically.

The present study has only considered one Reynolds number and diameter ratio. Future works of varying the Reynolds number and diameter ratio might give better insight of effect of swirling motion on impinging annular jet heat transfer.

REFERENCES

ICHIMIYA, K. 2003. Heat transfer characteristics of an annular turbulent impinging jet with a confined wall measured by thermosensitive liquid crystal. Heat and mass transfer, 39, 545-551.

KALININA, S., TEREKHOV, V. & SHAROV, K. 2015. Special features of flow in an annular jet impinging on a barrier. Fluid Dynamics, 50, 665-671.

LASCHEFSKI, H., CZIESLA, T., BISWAS, G. & MITRA, N. 1996. Numerical investigation of heat transfer by rows of rectangular impinging jets. Numerical Heat Transfer, Part A Applications, 30, 87-101.

LEE, D. H., WON, S. Y., KIM, Y. T. & CHUNG, Y. S. 2002. Turbulent heat transfer from a flat surface to a swirling round impinging jet. International Journal of Heat and Mass Transfer, 45, 223-227.

MAKI, H. & ITO, J. Heat transfer on radial wise wall jet and annular stagnation line by an annular impinging jet. Proceedings of JSME Conference on Mechanics and Materials, 1979. 146-153.

MAKI, H. & YABE, A. 1989. Heat transfer by the annular impinging jet. EXPERIMENTAL HEAT TRANSFER An International Journal, 2, 1-12.

MUSIKA, W., WAE-HAYEE, M., VESSAKOSOL, P., NIYOMWAS, B. & NUNTADUSIT, C. Investigation of Flow and Heat Transfer Characteristics of Annular Impinging Jet. Advanced Materials Research, 2014. Trans Tech Publ, 1223-1227.

YANG, H., KIM, T., LU, T. & ICHIMIYA, K. 2010. Flow structure, wall pressure and heat transfer characteristics of impinging annular jet with/without steady swirling. International Journal of Heat and Mass Transfer, 53, 4092-4100.